



Dinuclear platinum(II) complexes of imidazophenanthroline-based bridging ligands as potential anticancer agents: synthesis, characterization, and in vitro cytotoxicity studies

Carlson Alexander¹ · N. U. Prajith¹ · P. V. Priyanka¹ · A. Nithyakumar¹ · N. Arockia Samy¹

Received: 30 October 2018 / Accepted: 27 March 2019
© Society for Biological Inorganic Chemistry (SBIC) 2019

Abstract

The synthesis and characterization of the dinucleating ligands 1,2-bis(2-(1*H*-imidazo[4,5-*f*][1,10]phenanthrolin-2-yl)phenoxy)ethane (**L1**) and 1,2-bis(2-(1*H*-imidazo[4,5-*f*][1,10]phenanthrolin-2-yl)phenoxy)hexane (**L2**) and their dinuclear complexes [Pt₂(**L1**)Cl₄] (**1**) and [Pt₂(**L2**)Cl₄] (**2**) and the in vitro cytotoxicity of the complexes against HeLa, HepG2, and MCF-7 cell lines are reported. Ligand **L1** crystallizes in the orthorhombic system with the space group *Pbca*. The complexes **1** and **2** undergo aquation following first-order kinetics. The MTT and trypan blue assays indicate higher cytotoxicity of the complexes towards the HepG2 and MCF-7 cell lines compared to cisplatin. The AO/EB assay and flow cytometry by Annexin V alexa fluor[®] 488/PI double staining assay demonstrate distinct morphological changes of apoptosis in a dose dependent manner. The cell cycle analysis shows a marked decrease in the DNA content in the G0/G1 phase with an increase in the G2/M phase on increasing the concentration of the complexes. The potential of the complexes as anticancer agents is demonstrated by their antiproliferative activity on the cell lines. The complexes interact with the major groove of DNA through H-bonding between the imidazole N–H protons and the nucleotide residues DC⁺21/N4 (cytosine) for complex **1** and DT⁺7/O2 (thymine) and DT⁺19/O2 (thymine) for complex **2**, with the binding energy of – 1.98 and – 4.45 kcal/mol, respectively.

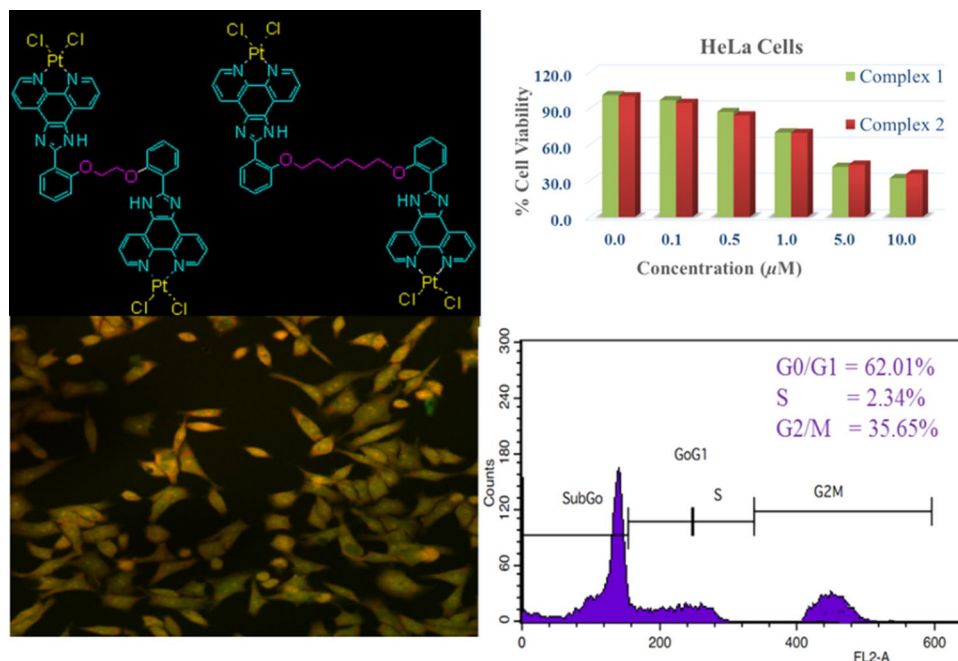
Electronic supplementary material The online version of this article (<https://doi.org/10.1007/s00775-019-01656-3>) contains supplementary material, which is available to authorized users.

✉ N. Arockia Samy
narockiasamy@loyolacollege.edu; narockiasamy@gmail.com
Carlson Alexander
carlson.alexander@chem.ox.ac.uk

¹ Department of Chemistry, Loyola College, Chennai 600034, India

Graphical Abstract

Dinuclear Pt(II) complexes of imidazophenanthroline-based dinucleating ligands exhibit antiproliferative activity against HeLa, HepG2, and MCF-7 cell lines



Keywords Anticancer drug · Apoptosis · DNA damage · Docking · Dinuclear platinum complexes · Imidazophenanthroline

Introduction

Since the serendipitous discovery of the inhibition of cell division in *E. coli* by cisplatin [1] and the subsequent discovery of its antitumor properties [2] by Rosenberg and his co-workers it has become the most prominent drug in cancer chemotherapy. Cisplatin is an effective drug used in nearly 50% of all cancer patients and a forerunner in the treatment of at least 18 distinct types of tumors [3]. However, despite its clinical impact, it induces a number of toxic side effects [4] and certain cancers are resistant to cisplatin therapy. In an attempt to develop a less toxic platinum anticancer drug carboplatin was introduced into the clinic in mid-1980s [5]. Compared with cisplatin, it is essentially devoid of nephrotoxicity, less toxic to the gastrointestinal tract, and less neurotoxic and widely used for the treatment of many types of cancer. Oxaliplatin, the third platinum anticancer drug approved by the FDA in 2002, shows a differing pattern of sensitivity to that of cisplatin [6] and is active against some cancer cells with acquired resistance to cisplatin [7].

Nedaplatin is used to treat cancers of the head, neck, esophagus, and small-cell- and non-small-cell lung cancers in Japan [8, 9]. Heptaplatin is approved for use in Korea for the treatment of gastric cancer. Lobaplatin is approved

for the treatment of chronic myelogenous leukemia, small-cell lung cancer, and metastatic breast cancer in China [10]. Satraplatin, also known as JM216, an orally active version of carboplatin [11], shows activity in human cancer cells with acquired cisplatin resistance [12]. Picoplatin, also known as JM473, retains activity against a range of cisplatin- and oxaliplatin-resistant cells in vivo [13]. The discovery and the development of cisplatin [14], the mechanisms of cisplatin resistance [15], the synthetic strategies [16] and mechanism of action [17–20] of platinum anticancer complexes, the status of platinum anticancer drugs in the clinic and in clinical trials [8], the resurgence of platinum-based cancer chemotherapy [21] the state-of-play and future of platinum drugs [22], and the ongoing effort for the development of next generation platinum drugs [23] are reviewed.

There are extensive evidence that platinum drugs exert their cytotoxic effects via the formation of platinum-DNA adducts [24–26]. The bifunctional platinum-DNA cross-links induce significant structural distortion in the double-helix of DNA and impede cellular processes such as replication and transcription leading to apoptosis and cell death [27]. Though cisplatin is widely used its efficiency against majority of the malignancies is highly limited due to its poor circulation and delivery to the tumor as well as deactivation

mechanisms. Another main problem associated with the use of the commercially available platinum complexes is the severe side effects arising from the lack of selectivity toward tumor cells [18].

In an attempt to overcome the platinum resistance in cancer chemotherapy ‘non-classical’ platinum complexes [28] which include *trans*-platinum complexes and polynuclear complexes capable of forming a different range of DNA adducts and display a different spectrum of anticancer activity compared to cisplatin and its analogs are developed. *trans*-Platinum complexes of the general formula *trans*-[PtCl₂(NH₃)L] (where L is a bulky, planar *N*-donor ligand) have been reported to be active in vitro and in vivo [29, 30]. Polynuclear complexes containing two or more metal centers covalently connected via appropriate linkers have emerged as a promising class of anticancer compounds with the ability to overcome resistance in chemoresistant cancers via new modes of action with the biomolecular targets. A host of dinuclear complexes containing *trans*-[PtCl_n(NH₃)_{3-n}] units bridged by alkanediamine linkers of variable length to facilitate flexible intra- and interstrand DNA cross-links have been reported by Farrell and his co-workers [31–34] and reviewed by Wheate and Collins [35, 36]. The unconventional DNA adducts enable diplatinum complexes to overcome cisplatin resistant ovarian cancer cells [34]. The binding of polynuclear platinum complexes with DNA is vastly different from that of cisplatin and is generally characterized by flexible, non-directional DNA adducts, formation of a greater percentage of interstrand to intrastrand adducts, and the ability to induce DNA conformational changes [37, 38].

Platinum complexes of polypyridine ligands capable of intercalating with DNA have also been studied for their anti-tumor activities [39–42]. Aldrich-Wright and her co-workers [43, 44] have studied dinuclear platinum complexes containing planar polyaromatic ligands which interact with DNA

by intercalation as anticancer agents. To improve the DNA binding capabilities of platinum drugs we have undertaken a research project on the development of dinuclear Pt(II) complexes of imidazophenanthroline-based ligands bridged by alkane linkers of different chain length. Herein we report the syntheses, characterization, and in vitro cytotoxicity studies of two dinuclear platinum(II) complexes (Fig. 1).

Experimental section

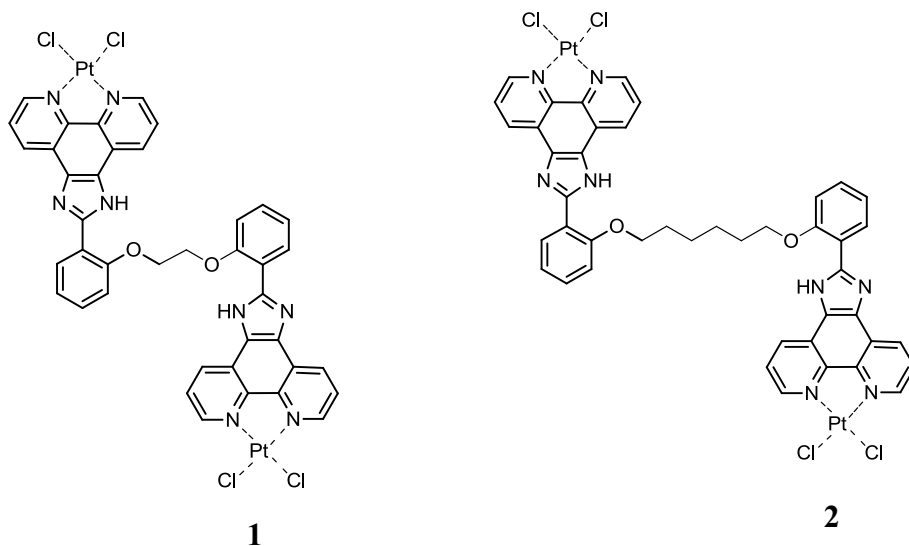
Materials for in vitro assays

All reagents and plastic wares used for aseptic works were either purchased sterile or sterilized according to literature recommendations. Propidium iodide, RNase A, MTT, DMSO (Hybri-Max™ sterile-filtered), trypan blue, and paraformaldehyde (Sigma-Aldrich); Dulbecco's phosphate buffer saline (PBS) (Himedia); agarose-type 1 and EDTA (Merck); acridine orange and ethidium bromide (Loba Chemie Pvt. Ltd.); minimum essential medium (MEM), trypsin (1:250), fetal bovine serum (FBS), and antibiotic/antimycotic, 100X (Gibco); DNA ladder (100 bp), proteinase K solution (20 mg/mL), Annexin V alexa fluor® 488/propidium iodide dead cell apoptosis kit (Invitrogen); and DNA gel loading dye (6X) (Thermo Scientific) were procured and stored according to the specifications.

Physical measurements

Infrared spectra were recorded on a Bruker Tensor II FT-IR Spectrometer operated by Opus 7.5 software package in the range of 4000–400 cm^{−1}. Spectra of the solid

Fig. 1 Structure of the complexes [Pt₂(L1)Cl₄] (1) and [Pt₂(L2)Cl₄] (2)



samples were recorded by making transparent potassium bromide (FT-IR grade, Fluka) pellets. CHN microanalyses were carried out using a Perkin Elmer 2400 Series II CHNS/O elemental analyzer interfaced with a Perkin Elmer AD 6 Autobalance. Helium (99.999%) was used as the carrier gas. The electrospray ionization (ESI) mass spectra were recorded on a Micromass Quattro II Triple Quadrupole mass spectrometer. The sample was dissolved in a suitable solvent such as methanol, acetonitrile, or water and introduced into the ESI source through a syringe pump at the rate of 5 μ L per min. The ESI capillary was set at 3.5 kV and the cone voltage at 40 V. The average spectrum of 6–8 scans was printed. NMR spectra were recorded on a Bruker AVANCE III 500 MHz (AV 500) multinuclear NMR spectrometer at 25 °C. The ^{13}C NMR spectra were recorded at 125 MHz at 25 °C and a standard 5 mm probe was used for the ^1H and ^{13}C NMR measurements. Spectra were recorded in CDCl_3 (99.9 atom % D) or $\text{DMSO}-d_6$ (99.90 atom % D) (Aldrich). The electronic absorption spectra were recorded on a Shimadzu UV-2450 UV–visible spectrophotometer controlled by the UV Probe version-2.33 software. The spectra were recorded in the region 190–800 nm in methanol or *N,N*-dimethyl formamide at 25 °C using a matched pair of Teflon-stoppered quartz cell of path length 1 cm. Solvent corrections were carried out before recording the spectra. Buchi Rotavapor (Model R-215) was used to remove the solvent and isolate the products at low temperature and pressure. Heto Holton cryogenic circulator bath (−45 °C) was used to carry out the reactions at low temperature. The circulating bath was filled with water-ethylene glycol (3:2 v/v) for a bath temperature of −10 °C and pure methanol for −45 °C.

X-ray diffraction data was collected with Bruker AXS Kappa Apex II CCD Diffractometer equipped with graphite monochromated Mo ($K\alpha$) ($\lambda = 0.7107 \text{ \AA}$) radiation. Crystal of suitable size fixed at the tip of the glass fiber using cyanoacrylate adhesive was mounted on the goniometer head with the aid of video microscope and optically centered at the goniometer axes. The automatic cell determination routine with 36 frames at three different orientations of the detector was employed to collect reflections for unit cell determination. Further, intensity data for structure determination were collected through an optimized strategy which gave an average fourfold redundancy. The structures were solved by direct methods using SIR92 and refined by full-matrix least squares techniques using SHELXL-2014 computer program. Molecular graphics were drawn using ORTEP3. Hydrogens on all carbon atoms were fixed at calculated positions and refined as riding model with $\text{C-H} = 0.9 \text{ \AA}$, $\text{Uiso}(\text{H}) = 1.2 \text{ Ueq}(\text{C})$, whereas hydrogens on nitrogen and water oxygen were fixed from the difference electron density peaks and allowed to refine freely.

Synthesis of organic precursors

1,10-Phenanthroline-5,6-dione

This compound was synthesized by the procedure reported by Yamada et al. [45]. A mixture of 1,10-phenanthroline (6.94 g, 35 mmol) and potassium bromide (41.65 g, 350 mmol) was taken in a round bottom flask, placed in an ice bath, and concentrated sulphuric acid (140 mL) was added in small portions followed by the addition of concentrated nitric acid (70 mL) to get a homogenous solution. The resulting solution was heated for 2 h at 85 °C, cooled to room temperature, poured into water (2.5 L), neutralized with sodium hydrogen carbonate, and extracted with chloroform. The chloroform extract was flash evaporated and the resulting solid product was recrystallized in hot methanol to obtain yellow needles, yield 3.97 g (54%), mp 271 °C. Anal. Calcd for $\text{C}_{12}\text{H}_6\text{N}_2\text{O}_2$ ($M_r = 210.19$): C, 68.57; H, 2.88; N, 13.33. Found: C, 68.37; H, 2.70; N, 13.32%. IR (KBr, cm^{-1}): 3061 $\nu_s(\text{C-H})$ (aromatic), 1685 $\nu_s(\text{C=O})$, 1575 $\nu_s(\text{C=N})$, 1460 and 1414 $\nu_s(\text{C=C})$, 739 $\delta(\text{C-H})$. ^1H NMR (500 MHz, CDCl_3 , 298 K): δ 7.50 (d, 2H, $J = 3.5 \text{ Hz}$, $-\text{N-CH-CH-}$), 8.37 (d, 2H, $J = 7 \text{ Hz}$, $-\text{PyH}$), 8.98 (s, 2H $-\text{N-CH-}$). ^{13}C NMR (125 MHz CDCl_3 , 298 K): δ 125.5, 127.9, 137.1, 152.7, 156.2, 178.5. FAB MS: m/z 210 $[\text{M}]^+$.

2,2'-(Ethane-1,2-diylbis(oxy))dibenzaldehyde

It was synthesized by modifying the procedure reported by Armstrong and Lindoy [46]. To a solution of salicylaldehyde (5.0 mL, 48 mmol) in ethanol (30 mL) was added a solution of sodium hydroxide (2 g, 50 mmol) in water (100 mL), warmed, and 1,2-dibromoethane (2.0 mL, 24 mmol) was added followed by ethanol (20 mL) to get a homogeneous solution. The solution was refluxed under argon atmosphere for 100 h, cooled to 0 °C, and the colorless needles that separated out were filtered, washed with water, dried, and recrystallized in ether–chloroform (1:1 v/v), yield 3.70 g (57%). Anal. Calcd for $\text{C}_{16}\text{H}_{14}\text{O}_4$ ($M_r = 270.28$): C, 71.10; H, 5.22. Found: C, 71.02; H, 5.10%. IR (KBr, cm^{-1}): 2869 $\nu_s(\text{C-H})$, 1239 $\nu_{as}(\text{C-O-C})$, 1061 $\nu_s(\text{C-O-C})$, 756 $\delta(\text{C-H})$ (aromatic), 2922 $\nu_{as}(\text{C-H})$, 2866 $\nu_s(\text{C-H})$ (aliphatic), 1687 $\nu_s(\text{C=O})$, 1485 and 1452 $\nu_s(\text{C=C})$ (aromatic ring), 756 $\delta(\text{C-H})$. ^1H NMR (500 MHz, CDCl_3 , 298 K): δ 10.45 (s, 2H, $-\text{CHO}$), 7.86 (d, 2H, $J = 7.5 \text{ Hz}$, H_2), 7.09 (t, 2H, $J = 8.5 \text{ Hz}$, H_3), 7.59 (t, 2H, $J = 7.7 \text{ Hz}$, H_4), 7.07 (d, 2H, $J = 8.5 \text{ Hz}$, H_5), 4.54 (s, 4H, $-\text{O-CH}_2-$). ^{13}C NMR (125 MHz, CDCl_3 , 298 K) δ 67.0, 112.8, 121.4, 125.2, 128.6, 135.9, 160.7, 189.3. MS: m/z 271 $[\text{M}]^+$.

2,2'-(Hexane-1,6-diylbis(oxy))dibenzaldehyde

To a solution of salicylaldehyde (5.0 mL, 48 mmol) in ethanol (30 mL) was added a solution of sodium hydroxide (2 g, 50 mmol) in water (100 mL) and refluxed for 30 min. A solution of 1,6-dibromohexane (3.7 mL, 24 mmol) in ethanol (10 mL) was added dropwise to the reaction mixture and refluxed for 100 h under argon atmosphere. The solvent was flash evaporated to dryness, the residue was washed with water, and recrystallized in ether to give colorless needles, yield 4.00 g (51%). Anal. Calcd for $C_{20}H_{22}O_4$ ($M_r = 326.39$): C, 73.60; H, 6.79. Found: C, 73.55; H, 6.77%. IR (KBr, cm^{-1}): 3420 ν_s (N–H), 2852 ν_s (C–H) (aliphatic), 1682 ν_s (C=O), 1487 and 1456 ν_s (C=C) (aromatic ring), 1247 ν_{as} (C–O–C), 1036 ν_s (C–O–C), 760 δ (C–H). 1H NMR (500 MHz, $CDCl_3$, 298 K): δ 1.59 (q, 4H, $-CH_2-$), 1.92 (q, 4H, $-CH_2-$), 4.1 (t, 4H, $J = 6.5$ Hz, $-O-CH_2-$), 10.50 (s, 2H, $-CHO$), 7.82 (d, 2H, $J = 7.5$ Hz, H_2), 7.01 (d, 2H, $J = 7.5$ Hz, H_3), 7.52 (t, 2H, $J = 7$ Hz, H_4), 6.96 (t, 2H, $J = 8.5$ Hz, H_5). ^{13}C NMR (125 MHz, $CDCl_3$, 298 K): δ 25.8, 29.0, 68.2, 112.5, 120.5, 128.2, 124.8, 135.9, 161.4, 189.7. ESI-MS: m/z 328 $[M + H]^+$.

Synthesis of 1,2-bis(2-(1*H*-imidazo[4,5-*f*][1,10]phenanthrolin-2-yl)phenoxy)ethane (L1) and 1,6-bis(2-(1*H*-imidazo[4,5-*f*][1,10]phenanthrolin-2-yl)phenoxy)hexane (L2)

General procedure

A solution of 2,2'-(ethane-1,2-diylbis(oxy))dibenzaldehyde (1.00 g, 3.7 mmol) (for **L1**) and 2,2'-(hexane-1,6-diylbis(oxy))dibenzaldehyde (1.21 g, 3.7 mmol) (for **L2**) in acetic acid was added to a hot solution of 1,10-phenanthroline-5,6-dione (2.10 g, 10 mmol) and ammonium acetate (15.42 g, 200 mmol) in acetic acid (180 mL) under stirring and refluxed for 12 h under an argon atmosphere. The reaction mixture was cooled to room temperature, transferred into a beaker containing 200 mL water, and neutralized by the drop wise addition of aqueous ammonia (25%) with stirring. The yellow product that separated out was filtered, washed with water, and dried in vacuo.

L1. Recrystallized in methanol to obtain yellow crystals, yield 1.90 g (79%). Anal. Calcd for $C_{40}H_{26}N_8O_2$ ($M_r = 650.69$): C, 73.84; H, 4.03; N, 17.22. Found: C, 73.80; H, 4.02; N, 17.20%. IR (KBr, cm^{-1}): 3386 ν_s (N–H), 1235 ν_{as} (C–O–C), 1057 ν_s (C–O–C), 1607 ν_s (C=N), 805 γ (C–H) (pyridine ring). 1H NMR (500 MHz, $DMSO-d_6$, 298 K): δ 4.90 (s, 4H, $-O-CH_2-$), 7.83 (d, 2H, $J = 7.5$ Hz, H_2), 7.45 (t, 4H, $J = 8.5$ Hz, H_3), 7.05 (t, 4H, $J = 8.0$ Hz, H_4), 7.50 (d, 2H, $J = 7.0$ Hz, H_5), 11.50 (s, 2H, $-NH$), 7.95 (d, 2H, $J = 8.5$ Hz, H_7), 7.25 (t, 4H, $J = 8.0$ Hz, H_8), 8.78 (d, 2H, $J = 9.5$ Hz, H_9). ^{13}C NMR (125 MHz, $DMSO-d_6$, 298 K): 113.9, 119.2,

121.8, 122.6, 129.2, 131.2, 143.5, 147.3, 147.5, 156.1. ESI-MS: m/z 651 $[M]^+$.

L2. Purified by column chromatography using acetone–acetonitrile–acetic acid (5:4:1 v/v) as the eluent. The yellow powder obtained was washed with water and dried in vacuo to get bright yellow powder, yield 1.49 g (57%). Anal. Calcd for $C_{44}H_{34}N_8O_2$ ($M_r = 706.79$): C, 74.77; H, 4.85; N, 15.85. Found: C, 74.69; H, 4.81; N, 15.80%. IR (KBr, cm^{-1}): 3412 ν_s (N–H), 3060 ν_s (C–H), 2937 ν_s (C–H), 1607 ν_s (C=N), 1239 ν_s (C–O–C), 1091 ν_s (C–O–C), 740 δ (C–H). 1H NMR (500 MHz, $DMSO-d_6$, 298 K): δ 1.44 (q, 4H, $-CH_2-$), 1.76 (q, 4H, $-CH_2-$), 3.99 (t, 4H, $-O-CH_2-$), 6.99 (d, 2H, $J = 7.5$ Hz, H_4), 7.38 (m, 2H, H_5), 7.10 (m, 2H, H_6), 8.05 (d, 2H, $J = 7.0$ Hz, H_7), 13.12 (s, 2H, $-NH$), 8.89 (d, 4H, $J = 7.5$ Hz, H_9), 7.75 (m, 4H, H_{10}), 8.96 (m, 4H, H_{11}). ^{13}C NMR (125 MHz, $DMSO-d_6$, 298 K): δ 156.3, 149.4, 146.7, 131.7, 131.6, 130.4, 130.3, 124.6, 121.1, 113.0, 69.0, 28.8, 26.4. ESI-MS: m/z 706 $[M]^+$.

Synthesis of dinuclear platinum(II) complexes [Pt₂(L1)Cl₄] (1) and [Pt₂(L2)Cl₄] (2)

General procedure

1,2-Bis(2-(1*H*-imidazo[4,5-*f*][1,10] phenanthrolin-2-yl)phenoxy)ethane (**L1**) (0.65 g, 1 mmol) (for **1**) and 1,6-bis(2-(1*H*-imidazo[4,5-*f*][1,10] phenanthrolin-2-yl)phenoxy)hexane (**L2**) (0.71 g, 1 mmol) (for **2**) in hydrochloric acid (50 mL, 2 M) was added to a solution of potassium tetrachloroplatinate(II) (1.00 g, 2.4 mmol) in water (10 mL) and stirred for 8 h to give a yellow solid. This solid product was filtered, washed with water, and dried in vacuo.

[Pt₂(L1)Cl₄] (1). Recrystallized in DMF:methanol (1:1 v/v) to obtain a pale yellow crystalline solid, yield 0.60 g (51%). Anal. Calcd for $C_{40}H_{26}Cl_4N_8O_2Pt_2$ ($M_r = 1182.65$): C, 40.62; H, 2.21; N, 9.47. Found C, 40.60; H, 2.21; N, 9.38%. IR (KBr, cm^{-1}): 3396 ν_s (N–H), 1235 ν_{as} (C–O–C), 1057 ν_s (C–O–C), 926 γ (C–H) (pyridine ring), 740 δ (C–H). 1H NMR (500 MHz, $DMSO-d_6$, 298 K): δ 4.98 (m, 4H, $-O-CH_2-$), 7.17 (m, 2H, H_2), 7.63 (m, 2H, H_3), 7.51 (m, 2H, H_4), 8.16 (m, 2H, H_5), 12.38 (s, 2H, $-NH$), 8.82 (m, 4H, H_7), 7.74 (m, 4H, H_8), 9.30 (m, 4H, H_9). ESI MS: m/z 1180 $[M]^+$.

[Pt₂(L2)Cl₄] (2). Recrystallized in DMSO to obtain a pale yellow powder, yield 0.69 g (56%). Anal. Calcd for $C_{44}H_{34}Cl_4N_8O_2Pt_2$ ($M_r = 1238.76$): C, 42.66; H, 2.77; N, 9.05. Found C, 42.61; H, 2.76; N, 9.01%. IR (KBr, cm^{-1}): 3396 ν_s (N–H), 2926 ν_s (C–H) (aliphatic), 1234 ν_{as} (C–O–C), 1087 ν_s (C–O–C), 751 δ (C–H). 1H NMR (500 MHz, $DMSO-d_6$, 298 K): δ 1.23 (m, 4H, $-CH_2-$), 1.87 (m, 4H, $-CH_2-$), 4.10 (m, 4H, $-O-CH_2-$), 6.97 (m, 4H, H_4 and H_7), 7.46 (m, 2H, H_6), 7.67 (m, 2H, H_5), 9.30 (m, 4H, H_9), 12.90 (m, 2H,

–NH), 7.87 (m, 4H, H_{10}), 8.97 (m, 4H, H_{11}). MALDI-TOF: m/z 1201 $[M-Cl]^+$.

Kinetics of aquation

The kinetics of aquation of the complexes **1** and **2** were studied in water using an Agilent Cary 8454 UV–visible spectrophotometer operated by UV–Vis Chemstation software. Stock solutions of the complexes were prepared in DMSO (10 mM) and an aliquot (30 μ L) was diluted to 3 mL in water in a quartz cuvette and the UV–visible spectra of each solution was immediately recorded in the wavelength region 190–1100 nm at 1-min intervals. The wavelength at which the absorbance changes significantly with time was selected to monitor the changes in absorbance as a function of time for the determination of rate constant [47].

The time-dependent changes in the absorbance at selected wavelength were recorded at 30-s intervals. The absorbance versus time data for each complex was computer-fitted to the first-order rate equation (Eq. 1) using Origin Pro 8.5 software. The slope of the straight line gave the rate constant for aquation (k_{H_2O}) and the half-life period ($t_{1/2}$) was calculated using the k value (Eq. 2).

$$\ln A = \ln A_0 - kt \quad (1)$$

$$t_{1/2} = 0.6931/k \quad (2)$$

where A_0 and A are the absorbance at the start of the reaction and at time t , respectively.

Cell culture

The human breast cancer adenocarcinoma cell line MCF-7, human liver hepatocellular carcinoma cell line HepG2, and human cervical adenocarcinoma cell line HeLa were procured from the National Center for Cell Sciences, Pune, India. HeLa cells were maintained in GM-5 minimum essential medium (MEM, Gibco®) supplemented with 5% FBS (fetal bovine serum, Gibco®) and 1% Ab/Am (Antibiotic/antimycotic, 100X, Gibco™) and MCF-7 and HepG2 in GM-10 (MEM, 10% FBS, and 1% Ab/Am) at 37 °C, 95% humidity, and 5% CO₂. HeLa cells were passaged thrice while MCF-7 and HepG2 twice in a week.

In vitro cytotoxicity assays

Stock solutions of the platinum complexes **1** and **2** required for different assays were prepared in DMSO (sterile-filtered) and diluted with the growth media maintaining the final DMSO concentration of 0.2%. The concentration of DMSO in the treated and the control wells was kept the same. This concentration of DMSO (0.2%) was found to be non-toxic to the cell lines. The MTT and the trypan blue assays were carried out

using five concentrations of the complexes (0.1, 0.5, 1.0, 5.0, and 10.0 μ M) for 24 h.

Trypan blue exclusion assay

Cell viability using trypan blue assay was carried out by incubating cells (1×10^6 cells/well) with different concentrations (0.1, 0.5, 1.0, 5.0, and 10.0 μ M) of the complexes **1** and **2** in six-well plates at 37 °C for 3 h. The cells were harvested and centrifuged at 250× G for 5 min and resuspended in 100 μ L phosphate buffer saline (PBS). Trypan blue solution (100 μ L, 0.4%) was mixed with the above suspension and incubated at room temperature for 3 min. The live and dead cells were scored using a hemocytometer. The data were analyzed by plotting percentage of viable cells against concentration.

MTT assay and estimation of IC₅₀ values

The colorimetric MTT assay was performed to quantify the cytotoxicity of the complexes **1** and **2** on the cell lines. Cells (2×10^4 cells/well) were treated with five different concentrations (0.1, 0.5, 1.0, 5.0, and 10.0 μ M) of the complexes in triplicate in a 96-well plate in 150 μ L GM-10 per well, and incubated at 37 °C under 5% CO₂ and 95% humidity conditions for 48 h. GM-10 containing 0.2% DMSO was used as the negative control. After the incubation period, the supernatant media was replaced with 100 μ L MTT solution in PBS (0.75 mg/mL final concentration) and incubated at 37 °C for 4 h, and DMSO (100 μ L) was added to each well for solubilizing the MTT formazan crystals. After incubating at room temperature for 30 min, the absorbance was measured at 570 nm using an ELISA plate reader. The IC₅₀ values were obtained from the percentage cell viability versus log $[C]$ plot of the dose–response data.

AO/EB dual staining assay

The HeLa cells were seeded on sterile glass coverslips kept on six-well plates (10^5 cells/well) and incubated with different concentrations (1 and 5 μ M) of the complexes **1** and **2** at 37 °C for 24 h. The cells were then washed with PBS, fixed using paraformaldehyde (4% w/v), counter stained with 40 μ L of AO/EB solution (1 part 25 μ g/mL AO in PBS and one part 25 μ g/mL EB in PBS), washed thoroughly with PBS, and mounted on microscopic slide over 15% glycerol. Images were captured in line mode with 20× objective using a Zeiss LSM 700 laser scanning confocal microscope.

Annexin V alexa fluor® 488/propidium iodide apoptosis assay

The apoptotic/necrotic cells were quantified by flow cytometry using the Annexin V alexa fluor® 488/propidium iodide

dead cell apoptosis kit (Invitrogen™). The HeLa cells in a six-well plate (1×10^6 cells/well) were treated with different concentrations (1 and 5 μM) of the complexes **1** and **2** and incubated at 37 °C for 24 h. The cells were trypsinized, washed twice with ice cold PBS, and resuspended in 100 μL of 1X annexin V binding buffer. Annexin V alexa fluor® 488 (5 μL) and propidium iodide (1 μL , 100 $\mu\text{g/mL}$) were added to each sample and incubated at room temperature for 15 min. To this cell suspension was added 400 μL 1X annexin V binding buffer, gently mixed, and analyzed using Beckmann Coulter Moflo XDP cell sorter operated using summit 4.2 software.

Cell cycle analysis

HeLa cells with a cell density of 1×10^6 cells/mL were treated with 1.0 and 5.0 μM concentration of the complexes **1** and **2** at 37 °C for 24 h. Treated and untreated cells were harvested in 1.5 mL microcentrifuge tube, washed with PBS, and fixed with 1 mL of 70% ethanol at 4 °C for 30 min. Cells were then washed twice with 1 mL PBS solution, centrifuged at $850 \times G$ for 10 min, and discarded the supernatant carefully. The cell pellets were suspended in 0.2 mL PBS, treated with 50 μL RNase A solution (100 $\mu\text{g/mL}$), and incubated for 30 min at 37 °C. The suspension was mixed gently, treated with 200 μL of propidium iodide (50 $\mu\text{g/mL}$), and kept in the dark at 4 °C. The cell cycle distribution was measured using BD FACS Calibur™ flow cytometer and the data were analyzed using Cellquest Pro software.

Molecular docking study with DNA

The molecular docking study of the complexes **1** and **2** with DNA was performed using AutoDock 4.2 software and the AutoDock scoring function which is an interactive molecular graphics program for the interaction, docking calculations, and to identify possible binding sites of these biomolecules. The energy optimized structures of the platinum complexes as a .mol file were used as input for AutoDock software and were converted to .pdb format for performing the docking experiment. The crystal structure of DNA dodecamer (5'-CGCGAATTCGCG-3')₂ (PDB ID: 1BNA) was retrieved from the protein data bank (<http://www.rcsb.org/pdb>). The DNA was treated as a rigid target molecule and the platinum complexes as flexible ligand molecules. While preparing the receptor, the water molecules were removed and polar hydrogen atoms and the Gasteiger and Kollman partial atomic charges were added to the DNA. A grid box of $90 \times 90 \times 90$ dimension (total grid points per map of 753,571) and grid spacing 0.375 Å was developed for the docking experiment. The default docking parameters were set except the number of evaluations and the Lamarckian genetic algorithm runs which were set at 2.5 million and 10,

respectively. The lowest docked energy conformation was selected as the best binding mode. The docking interactions were visualized using PyMol 1.4.1 software.

Results and discussion

Synthesis and characterization of ligands

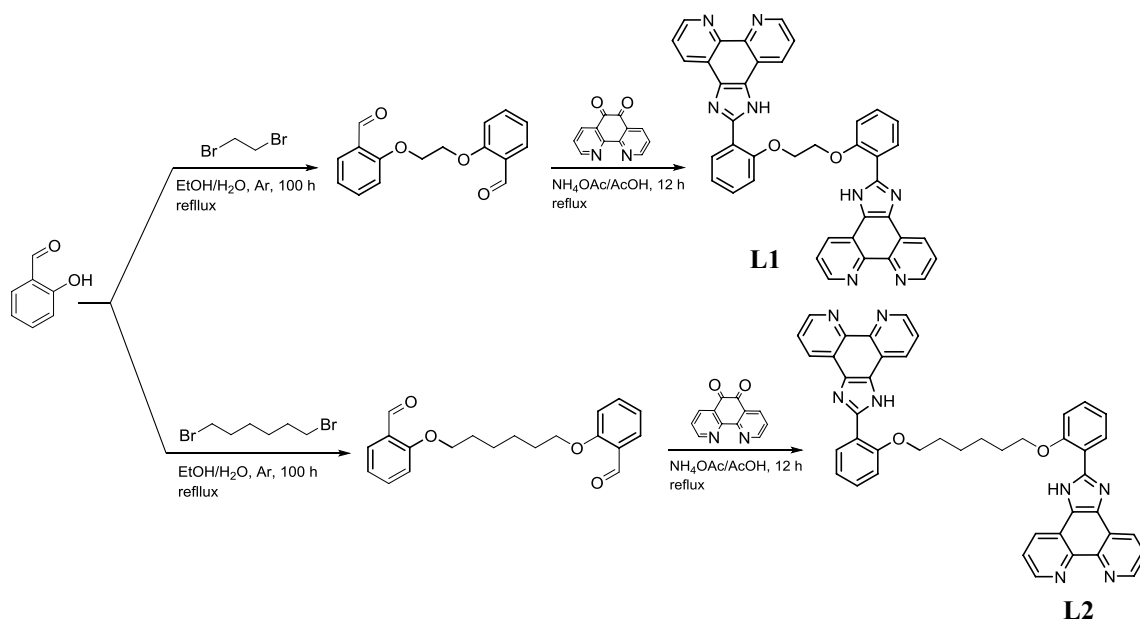
The condensation of 2,2'-(ethane-1,2-diylbis(oxy))dibenzaldehyde (1 equiv) and 2,2'-(1,6-hexanediybis(oxy))dibenzaldehyde with 1,10-phenanthroline-5,6-dione (2.4 equiv) in the presence of ammonium acetate (40 equiv) in acetic acid under argon atmosphere followed by neutralization with ammonia yields **L1** and **L2**, respectively (Scheme 1). The ESI mass spectrum of **L1** shows a peak at m/z 651 due to the molecular ion $[\text{M}]^+$. The electronic absorption spectrum of **L1** in methanol contains two absorption bands at 276 ($\epsilon = 60,200 \pm 33$ L/mol/cm) and 228 nm ($\epsilon = 63,000 \pm 56$ L/mol/cm) due to the $\pi-\pi^*$ transitions. The ESI mass spectrum of **L2** shows a peak at m/z 706 corresponding to the molecular ion $[\text{M}]^+$. The electronic absorption spectrum of **L2** in DMF contains absorption bands at 276 ($\epsilon = 30,118 \pm 46$ L/mol/cm) and 312 nm ($\epsilon = 19,308 \pm 32$ L/mol/cm) assignable to the $\pi-\pi^*$ transitions.

Synthesis and characterization of complexes

The reaction of the preformed ligands **L1** and **L2** with a solution of potassium tetrachloroplatinate(II) in hydrochloric acid (2 M) gives the complexes **1** and **2**, respectively. The ESI mass spectrum of **1** shows the molecular ion peak at m/z 1180 $[\text{M}]^+$. The electronic absorption spectrum in DMF shows bands at 280 ($\epsilon = 81,500 \pm 32$ L/mol/cm) and 314 nm ($\epsilon = 62,500 \pm 42$ L/mol/cm) assignable to the ligand centered $\pi-\pi^*$ transitions. The absorption band at 419 nm ($\epsilon = 7300 \pm 54$ L/mol/cm) is due to the MLCT transition. The MALDI-TOF mass spectrum shows a peak at m/z 1201 corresponding to the species $[\text{M}-\text{Cl}]^+$. The electronic absorption spectrum of **2** in DMF shows bands at 277 ($\epsilon = 49,100 \pm 64$ L/mol/cm) and 314 nm ($\epsilon = 39,300 \pm 50$ L/mol/cm) assignable to the $\pi-\pi^*$ transitions and a band at 407 nm ($\epsilon = 4500 \pm 46$ L/mol/cm) due to the MLCT transition. The ligand centered $\pi-\pi^*$ transitions are bathochromically shifted due to coordination to the metal ions.

Crystal structure of the ligand L1

The ligand **L1** crystallizes in the orthorhombic system with the space group *Pbca* with the unit cell dimensions: $a = 29.283(2)$ Å, $b = 17.8424(13)$ Å, $c = 14.2023(10)$ Å, $\alpha = \beta = \gamma = 90^\circ$, $V = 7420.4$ Å³, $Z = 8$. The ORTEP and the packing diagrams of the crystal structure illustrate zig-zag



Scheme 1 The synthetic pathway of the organic precursors and ligands **L1** and **L2**

arrangement of the molecules along the *b*-axis leading to a ladder-like structure stabilized by aromatic π -stacking interactions (C37–H—C6 3.290 Å, C36–H—C7 3.358 Å, and C24–H—C13 Å) between the phenyl group and the imidazophenanthroline aromatic rings of the neighboring molecules. The ORTEP representation of **L1** is presented in Fig. S10 (ESI). There also exists two weak intramolecular hydrogen bondings between the imidazophenanthroline NH hydrogen and the linker oxygen (N4–H—O1 2.580 Å and N7–H—O2 2.670 Å) stabilizing the bent geometry of the molecule. The packing diagram, ladder-like arrangement of molecules along the *b*-axis, aromatic stacking interactions between the neighboring molecules, and intramolecular hydrogen bonding are presented in Fig. S11 (ESI). The crystallographic data are shown in Table S1 (ESI).

Kinetics of aquation of complexes

The aquation of platinum complexes used as anticancer agents assumes importance since the seminal investigation by Lippard et al. [48] who reported that the biological mechanism of action of cisplatin involves binding of $[\text{PtCl}(\text{OH}_2)(\text{NH}_3)_2]^+$, the hemi-hydrolyzed product of cisplatin formed in vivo, with DNA to form monofunctional adduct. In this milieu, aquation of the complexes **1** and **2** are studied by monitoring the changes in absorbance with time. The electronic absorption spectra of the stock solutions of complexes **1** and **2** in DMSO diluted in water feature a strong band at 276 nm and the absorbance decreases gradually with time. In the case of complex **1** there is an isobestic point at 338 nm. The rates of aquation of the complexes **1** and **2**, determined

by UV–Vis spectroscopy at 298 K, follows first-order kinetics with the rate constants nearly ten and two times faster than that of cisplatin [49]. The time-dependent changes in the absorbance of the complexes **1** and **2** ($\lambda_{\text{max}} = 276$ nm) in water at 298 K are depicted in Fig. 2. The rate constants and $t_{1/2}$ values are given in Table 1.

Cytotoxicity studies

MTT assay

On treating the HeLa, HepG-2, and MCF-7 cells lines with 0.1, 0.5, 1, 5, and 10 μM solutions of the complexes **1** and **2** for 48 h at 37 °C high mortality rate is observed at 5.0 and 10 μM concentrations. The IC_{50} values of the complexes **1**, **2**, and cisplatin on these cell lines, listed in Table 2, shows higher lethality of the complexes towards the HepG2 and MCF-7 cell lines compared to cisplatin. The influence of the spacer length on in vitro anticancer activity has been reported for dinuclear Ru(II) [50, 51] and Au(I) [51] complexes where the cytotoxicity correlates to the lipophilicity, which increases with increasing linker length. However, in our present study, there is no significant change in the cytotoxicity with an increase in the linker length. This similarity in the antiproliferative activity of the complexes **1** and **2** could be attributed to the combined effect of the higher lipophilicity and DNA groove binding potential (vide infra) and a sixfold decrease in the rate of aquation of **2** compared to that of **1**. The cytotoxicity profiles of the complexes and cisplatin against the cell lines are presented in Fig. 3.

Fig. 2 Time dependent electronic absorption spectra for the aquation of **a** $[\text{Pt}_2(\text{L1})\text{Cl}_4]$ (**1**) and **b** $[\text{Pt}_2(\text{L2})\text{Cl}_4]$ (**2**) and time-dependence of the absorbance at 276 nm for the hydrolysis of **c** $[\text{Pt}_2(\text{L1})\text{Cl}_4]$ (**1**) and **d** $[\text{Pt}_2(\text{L2})\text{Cl}_4]$ (**2**) in aqueous solution at 298 K

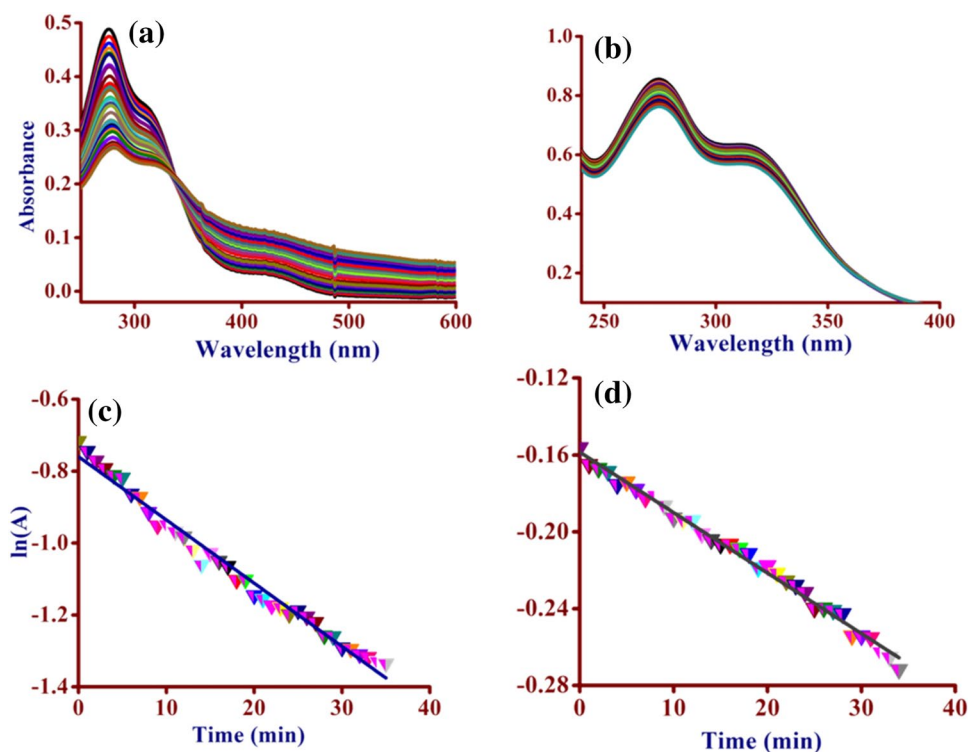


Table 1 The rate constants and $t_{1/2}$ values for the aquation of complexes

Complex	$k_{\text{H}_2\text{O}}$ ($10^{-5}/\text{s}$)	$t_{1/2}$ (min)
$[\text{Pt}_2(\text{L1})\text{Cl}_4]$ (1)	29.30	39.42
$[\text{Pt}_2(\text{L2})\text{Cl}_4]$ (2)	5.30	217.96

Table 2 IC_{50} value of the complexes **1** and **2** and cisplatin from MTT assay

Complex	HeLa cells	HepG-2 cells	MCF-7 cells
$[\text{Pt}_2(\text{L1})\text{Cl}_4]$ (1)	3.48 ± 1.9	3.67 ± 2.2	3.53 ± 2.4
$[\text{Pt}_2(\text{L2})\text{Cl}_4]$ (2)	3.29 ± 2.5	3.79 ± 3.0	3.67 ± 3.4
Cisplatin	2.62 ± 1.6	7.59 ± 0.9	15.18 ± 2.8

Trypan blue assay

Trypan blue exclusion assay is based on the principle that live cells which possess intact cell membranes will exclude the dye, whereas dead cells do not. Thus, when a cell suspension is treated with trypan blue viable cells will have clear cytoplasm, while nonviable cells a blue cytoplasm. In this study when the HeLa, HepG-2, and MCF-7 cell lines are treated with the complexes **1** and **2** at different concentrations (0.1, 0.5, 1, 5, and 10 μM) for 24 h at 37 °C a decrease in the cell proliferation is observed with increasing concentration of the complexes. At 5 and 10 μM concentrations

majority of the cells are damaged indicating lethality of the complexes towards the cell lines (Fig. 4).

Morphological assessment of apoptosis by AO/EB dual staining

The HeLa cell lines on treatment with the complexes **1** and **2** at 1 and 5 μM concentrations for 24 h at 37 °C and staining with AO/EB show distinct morphological changes of apoptosis as shown in Fig. 5. At 1 μM concentration of the complexes less apoptotic bodies are seen and the nuclei appear green, while at 5 μM concentration more apoptotic bodies with cell shrinkage and chromatin condensation are seen and the nuclei appear bright green. The control cell lines do not show any such morphological changes.

Flow cytometry by Annexin V alexa fluor® 488/PI double staining

Flow cytometry by Annexin V alexa fluor® 488 conjugate provides a quick and reliable detection method for studying the externalization of phosphatidylserine, one of the earliest indicators of apoptosis. The difference in the fluorescence intensity between apoptotic and nonapoptotic cells stained with the fluorescent Annexin V conjugates measured by flow cytometry is typically about 100-fold. It offers the possibility of detecting early phases of apoptosis before the loss of cell membrane integrity and permits measurements of the kinetics of apoptotic death in relation to the cell cycle. The

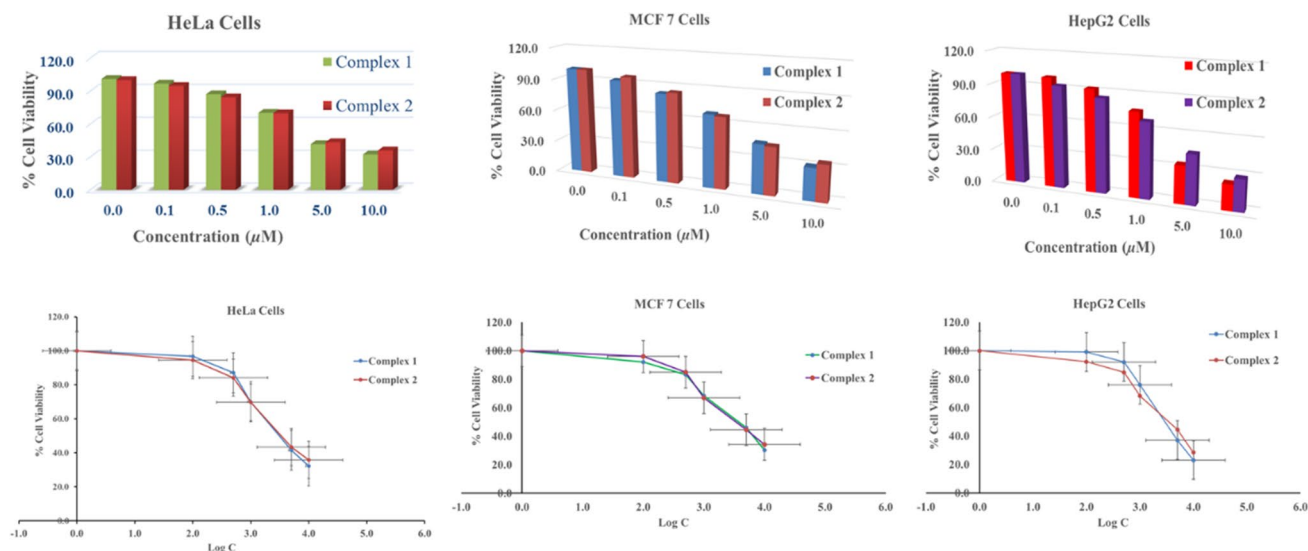


Fig. 3 MTT assay profiles of the HeLa, MCF-7, and HepG2 cell lines treated with different concentrations (0.1, 0.5, 1, 5, and 10 μM) of the complexes **1** and **2** for 24 h at 37 $^{\circ}\text{C}$

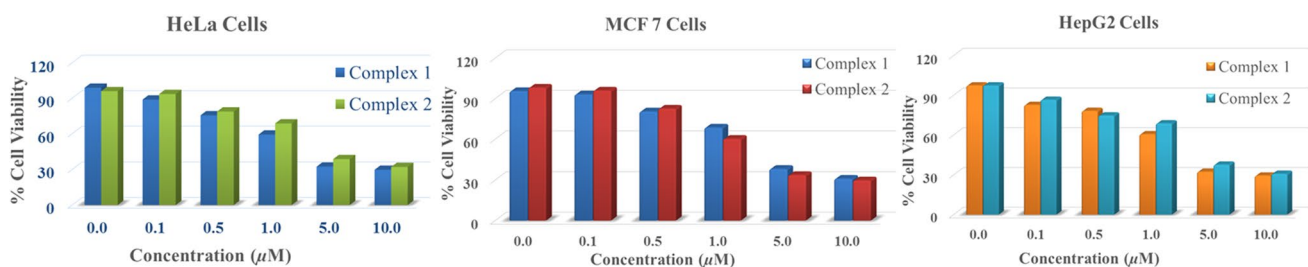


Fig. 4 Trypan blue assay: cytotoxicity profiles of the HeLa, MCF-7, and HepG2 cell lines incubated with different concentrations of the complexes **1** and **2** (0.1, 0.5, 1, 5, and 10 μM) for 24 h at 37 $^{\circ}\text{C}$

Annexin V conjugated alexa fluor[®] 488/PI binding assay is used to evaluate live cells, dead cells, and apoptotic and necrotic cells. Propidium iodide stains necrotic cells with red fluorescence, while the apoptotic cells show green fluorescence, dead cells show red and green fluorescence, and live cells show little or no fluorescence. When the HeLa cell lines are inoculated with the complexes **1** and **2** at 1 μM concentration for 24 h at 37 $^{\circ}\text{C}$ followed by staining with Annexin V alexa fluor[®] 488 and co-staining with PI, a significant apoptosis is observed with 21.26 and 22.63% live cells (R3) and 37.58 and 26.55% early apoptotic cells (R4), 25.63 and 35.37% late apoptotic cells (R2), and 15.55 and 15.45% nonviable cells (R1), respectively, compared to the control cells. At 5 μM concentration of the complexes a pronounced increase in apoptosis is observed with 17.26 and 11.35% viable cells (R3), 28.75 and 14.68% early apoptotic cells (R4), 36.35 and 51.52% late apoptotic cells (R2), and 17.63 and 22.44% dead cells (R1), respectively. The percentage of dead cells (R1), nonviable or necrotic cells (R2), viable or live cells (R3), and apoptotic cells (R4) are indicated in

Fig. 6. These results indicate that complex **2** induces more apoptosis than **1** at higher concentration which could be correlated to the higher lipophilicity of the former containing longer alkyl spacer. However, the IC_{50} values of the complexes **1** and **2** are comparable due to a sixfold decrease in the rate of aquation of **2** compared to that of **1**.

Cell cycle analysis by flow cytometry

The HeLa cell lines upon inoculation with 1 μM solution of the complexes **1** and **2** a marked decrease in the DNA content in the G0/G1 phase from 87.32 for the control to 69.38 and 66.41% and an increase in the G2/M phase from 7.90 to 26.97 and 29.82%, respectively, is observed. At 5 μM concentration of the complexes a rapid decrease in the DNA content in the G0/G1 phase from 87.32 for the control to 62.01 and 57.19% with an increase in the G2/M phase from 7.90 to 35.65 and 40.03%, respectively, is observed. On increasing the concentration of the complexes the DNA content in the G2/M phases increases indicating cell death

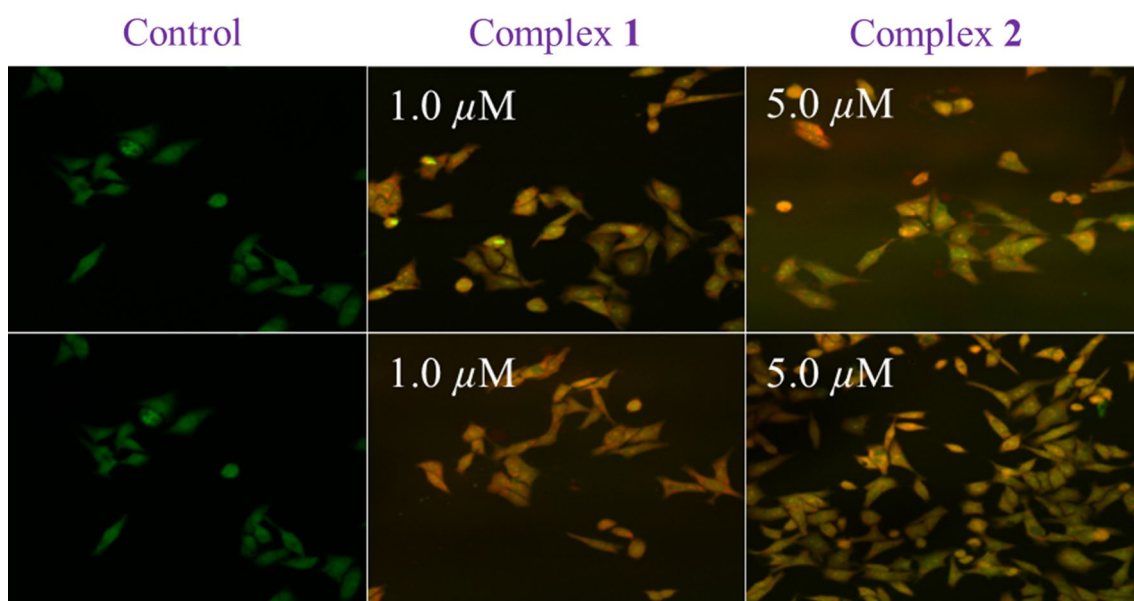


Fig. 5 Fluorescence microscopic images of the HeLa cell lines incubated with the complexes **1** and **2** (1 and 5 μM concentrations) for 24 h at 37 $^{\circ}\text{C}$ and stained with AO/EB

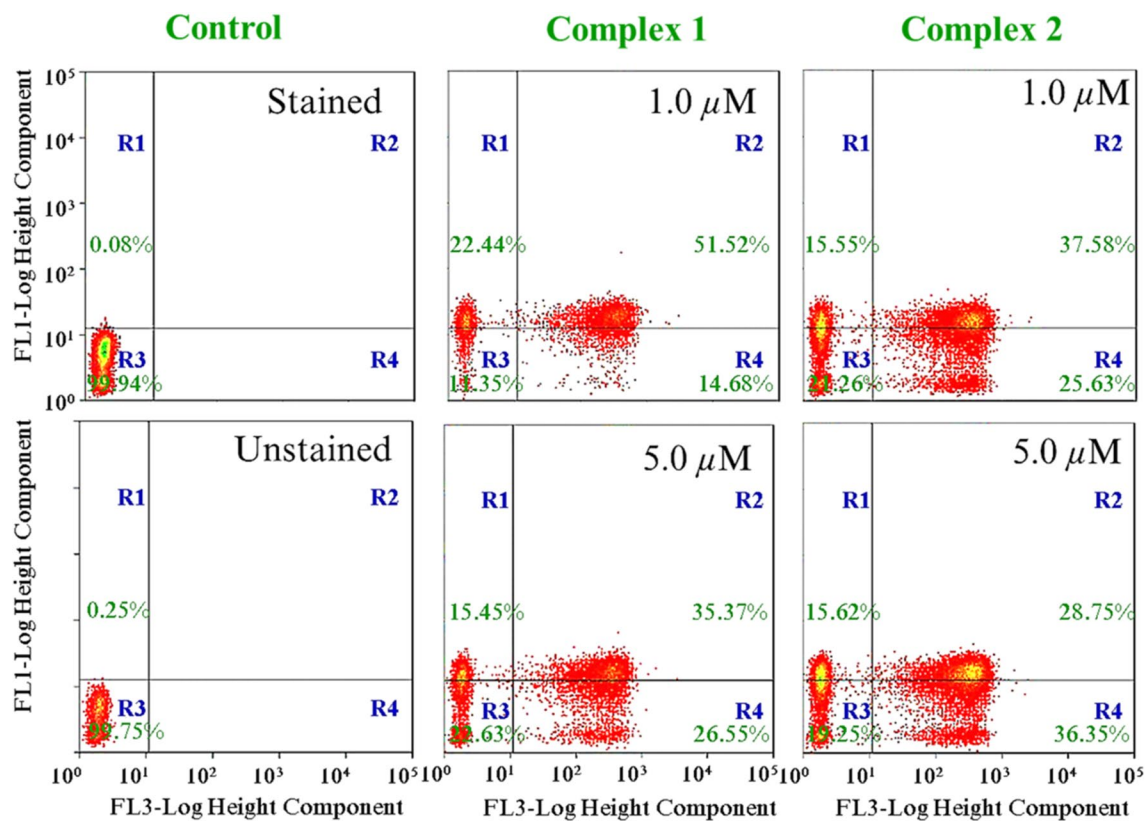


Fig. 6 Flow cytometry examination of HeLa cell lines after treatment with the complexes **1** and **2** for 24 h at 37 $^{\circ}\text{C}$ and staining with Annexin V alexa fluor[®] 488/PI (R1: dead cells, R2: nonviable or necrotic cells, R3: viable or live cells, and R4: apoptotic cells, percentage)

in a dose dependent manner. Our study demonstrates the potential of the complexes **1** and **2** as anticancer agents as they control the proliferation of the HeLa cells. The flow cytometry for the DNA quantification of HeLa cells after treating with the complexes followed by staining with PI is shown in Fig. 7.

Molecular docking study

The molecular docking study of the complexes **1** and **2** with DNA (PDB ID: 1BNA) is performed to evaluate the possible binding site, interaction mode, inhibition constant, desolvation energy, and binding affinity (the data are presented in Table 3). The complexes interact with DNA by hydrogen bonding at the major groove through the imidazole N–H protons of the complexes **1** and **2** and the nucleotide residues DC⁺21/N4 (cytosine) for **1** and DT⁺7/O2 (thymine) and DT⁺19/O2 (thymine) for **2** at the distances of 2.0 Å and 2.2 Å and 2.0 Å, respectively (Fig. 8). The relative binding energy of the docked complexes **1** and **2** with DNA are –1.98 and –4.45 kcal/mol, respectively. The inhibition constant and the desolvation energy also support the higher binding

potential of the complex **2** compared to **1**. Our study reveals that complex **2** binds efficiently with DNA than complex **1**.

Conclusion

Polynuclear platinum complexes represent a new class of anticancer drugs which could expand the realm of platinum chemotherapy treatment. Such complexes containing two or more platinum centers that can each covalently bind to DNA are capable of forming a completely different range of DNA adducts compared to cisplatin and its analogs. The synthetic strategy developed in this study could be exploited for the synthesis of a variety of imidazophenanthroline-based bridging ligands by changing the aldehyde precursors and linker moieties. The influence of the spacer length on the lipophilicity and DNA binding ability of the complexes could be exploited to develop dinuclear complexes with different linker moieties. The present study has the potential for studying the pH-dependent anticancer activity as the imidazophenanthroline-based bridging ligand contains ionisable N–H proton.

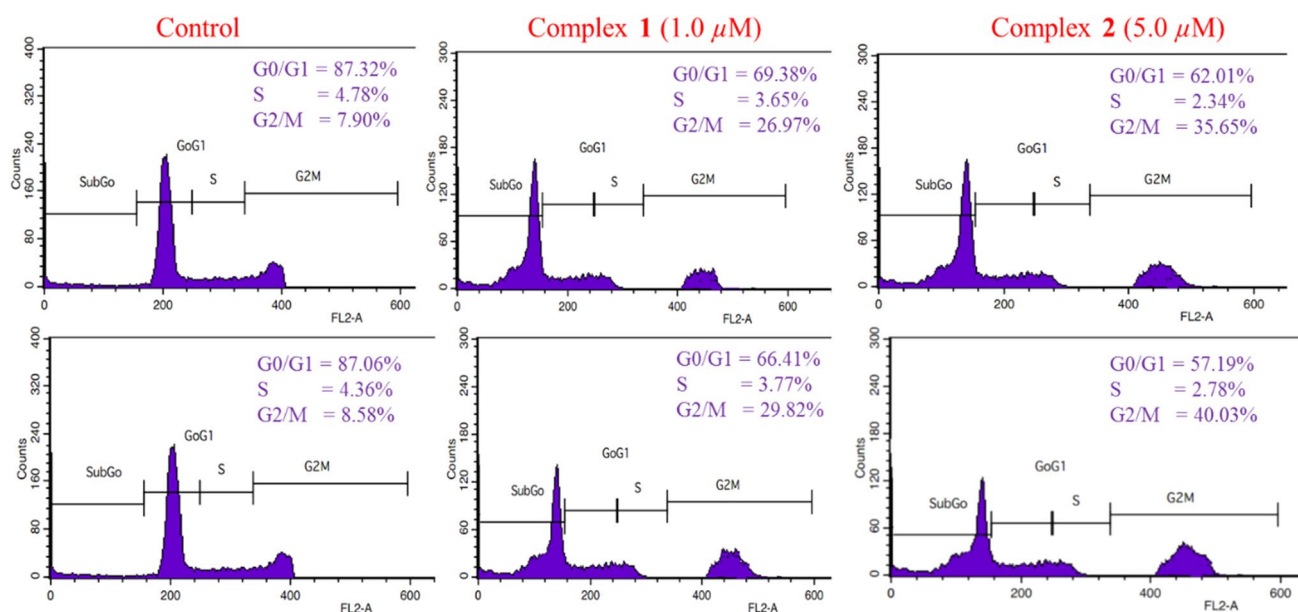


Fig. 7 Flow cytometry analysis of HeLa cell lines for DNA quantification after treating with the complexes **1** and **2** for 24 h at 37 °C and stained with PI

Table 3 Parameters of binding of the complexes **1** and **2** with DNA

Complex	Binding energy (kcal/mol)	Inhibition constant (mM)	Desolvation energy (kcal/mol)	Ligand efficiency
[Pt ₂ (L1)Cl ₄] (1)	–1.98	35.09	–5.26	0.03
[Pt ₂ (L2)Cl ₄] (2)	–4.45	0.55	–6.60	0.08

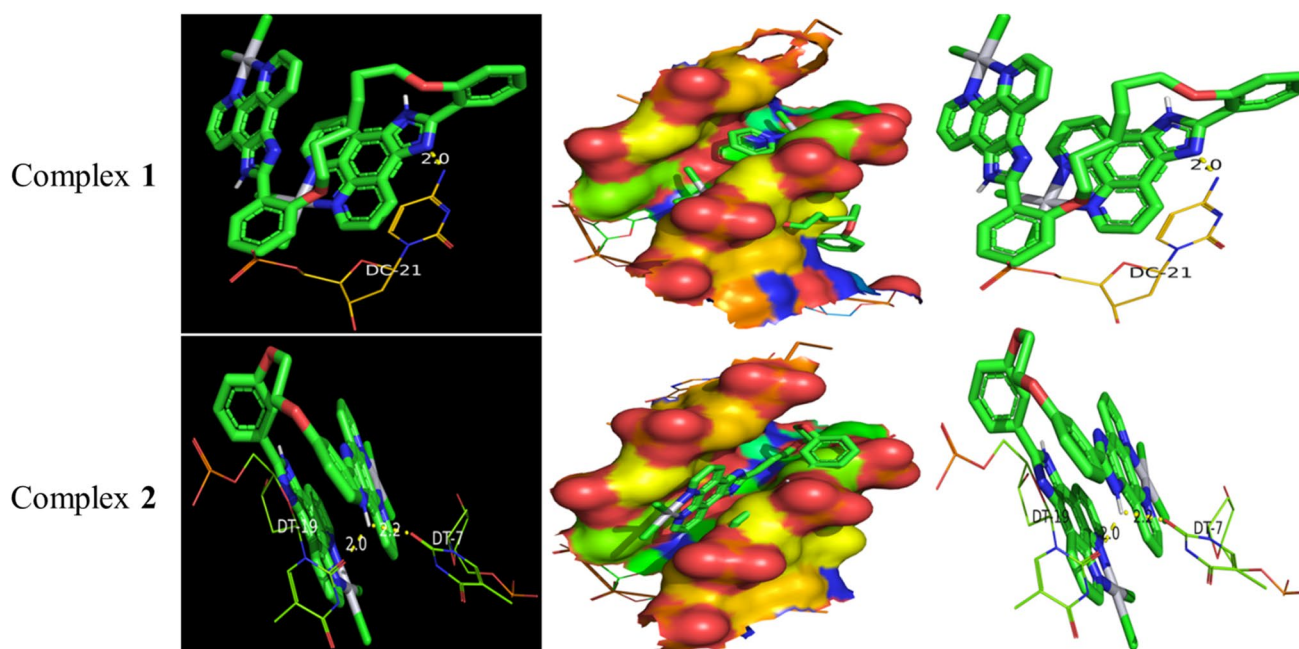


Fig. 8 Graphical representation of the interaction of complex **1** (top row) and **2** (bottom row) with DNA (PDB ID: 1BDNA)

Acknowledgements Partial financial support to Carlson Alexander from Loyola Research Park is gratefully acknowledged. NAS thanks SERB, New Delhi, for financial support. The service rendered by the Sophisticated Analytical Instrumentation Facilities (SAIF) at IIT-Madras and Punjab and Jawaharlal Nehru Universities for recording ESI-TOF and MALDI-TOF mass spectra and NMR spectra is gratefully acknowledged. We thank Dr. P. K. Sudhadevi Antharjanam, SAIF, IIT-Madras, Chennai, for her help in solving the crystal structure. We thank Dr. J. John Kirubakaran and Dr. S. Rajalakshmi, Department of Veterinary Microbiology, Madras Veterinary College, Chennai, for their invaluable help in carrying out the in vitro studies.

Compliance with ethical standards

Conflict of interest There are no conflicts to declare.

Appendix A: Supplementary data

ESI-TOF mass spectra, 500 MHz ^1H NMR spectra, and 125 MHz ^{13}C NMR spectra of organic precursors and the ligands **L1** and **L2**; crystal structure of **L1**, ESI-MS/MALDI-TOF MS and 500 MHz ^1H NMR spectra of the complexes.

References

- Rosenberg B, Vancamp L, Krigas T (1965) *Nature* 205:698–699
- Rosenberg B, Vancamp L, Trosko JE, Mansour VH (1969) *Nature* 222:385–386
- Chu E, DeVita VT Jr (2008) *Physician's cancer chemotherapy drug manual*. Jones and Bartlett Publishers, Sudbury
- Cvitkovic E (1998) *Cancer Treat Rev* 24:265–281
- Harrap KR (1985) *Cancer Treat Rev* 12:21–33
- Rixe O, Ortuzar W, Alvarez M, Parker R, Reed E, Paull K, Fojo T (1996) *Biochem Pharmacol* 52:1855–1865
- Raymond E, Faivre S, Chaney S, Woynarowski J, Cvitkovic E (2002) *Mol Cancer Ther* 1:227–235
- Wheate NJ, Walker S, Craig GE, Oun R (2010) *Dalton Trans* 39:8113–8127
- Shimada M, Itamochi H, Kigawa J (2013) *Cancer Manag Res* 5:67–76
- Welink J, Boven E, Vermorken JB, Gall HE, van der Vijgh WJF (1999) *Clin Cancer Res* 5:2349–2358
- Kelland LR, Abel G, McKeage MJ, Jones M, Goddard PM, Valenti M, Murrer BA, Harrap K (1993) *Cancer Res* 53:2581–2586
- Sharp SY, Rogers PM, Kelland LR (1995) *Clin Cancer Res* 1:981–989
- Sharp SY, O'Neill CF, Rogers PM, Boxall FE, Kelland LR (2002) *Eur J Cancer* 38:2309–2315
- Alderden RA, Hall MD, Hambley TW (2006) *J Chem Educ* 83:728–734
- Galluzzi L, Senovilla L, Vitale I, Michels J, Martins I, Kepp O, Castedo M, Kroemer G (2012) *Oncogene* 31:1869–1883
- Wilson JJ, Lippard SJ (2014) *Chem Rev* 114:4470–4495
- Jamieson ER, Lippard SJ (1999) *Chem Rev* 99:2467–2498
- Wang D, Lippard SJ (2005) *Nat Rev Drug Discov* 4:307–320
- Fuertes MA, Alonso C, Pérez JM (2003) *Chem Rev* 103:645–662
- Jung Y, Lippard SJ (2007) *Chem Rev* 107:1387–1407
- Kelland L (2007) *Nat Rev Cancer* 7:573–584
- Apps M, Choi E, Wheate N (2015) *Endocr Relat Cancer* 22:219–233
- Johnstone TC, Suntharalingam K, Lippard SJ (2016) *Chem Rev* 116:3436–3486
- Huang H, Zhu L, Reid BR, Drobny GP, Hopkins PB (1995) *Science* 270:1842–1845
- Takahara PM, Rosenzweig AC, Frederick CA, Lippard SJ (1995) *Nature* 377:649–652

26. Teuben JM, Bauer C, Wang AHJ, Reedijk J (1999) *Biochemistry* 38:12305–12312
27. Todd RC, Lippard SJ (2009) *Metallomics* 1:280–291
28. Lovejoy KS, Lippard SJ (2009) *Dalton Trans* 48:10651–10659
29. Farrell N, Kelland LR, Roberts JR, van Beusichem M (1992) *Cancer Res* 52:5065–5072
30. Kelland LR, Barnard CFJ, Mellish KJ, Jones M, Goddard PM, Valenti M, Bryant A, Murrer BA, Harrap KR (1994) *Cancer Res* 54:5618–5622
31. Billecke C, Finniss S, Tahash L, Miller C, Mikkelsen T, Farrell NP, Böglér O (2006) *Neuro Oncol* 8:215–226
32. Wu PK, Qu Y, Van Houten B, Farrell N (1994) *J Inorg Biochem* 54:207–220
33. Zou Y, Van Houten B, Farrell N (1994) *Biochemistry* 33:5404–5410
34. Yang D, van Boom SSGE, Reedijk J, van Boom JH, Farrell N, Wang AHJ (1995) *Nat Struct Biol* 2:577–578
35. Wheate NJ, Collins JG (2005) *Curr Med Chem Anticancer Agents* 5:267–279
36. Wheate NJ, Collins JG (2003) *Coord Chem Rev* 241:133–145
37. Brabec V, Kašpárková J, Vrána O, Nováková O, Cox JW, Qu Y, Farrell N (1999) *Biochemistry* 38:6781–6790
38. McGregor TD, Bousfield W, Qu Y, Farrell N (2002) *J Inorg Biochem* 91:212–219
39. Gao J, Woolley FR, Zingaro RA (2005) *J Med Chem* 48:7192–7197
40. Martinez R, Chacon-Garcia L (2005) *Curr Med Chem* 12:127–151
41. Khan QA, Kohlhagen G, Marshall R, Austin CA, Kalena GP, Kroth H, Sayer JM, Jerina DM, Pommier Y (2003) *Proc Natl Acad Sci* 100:12498–12503
42. Bolognese A, Correale G, Manfra M, Lavecchia A, Mazzoni O, Novellino E, Colla PL, Sanna G, Loddò R (2004) *J Med Chem* 47:849–858
43. Ang D, Harper BW, Cubo L, Mendoza O, Vilar R, Aldrich-Wright JR (2016) *Chem Eur J* 22:2317–2325
44. Harper BWJ, Aldrich-Wright JR (2015) *Dalton Trans* 44:87–96
45. Yamada M, Tanaka Y, Yoshimoto Y, Kuroda S, Shimao I (1992) *Bull Chem Soc Jpn* 65:1006–1011
46. Armstrong LG, Lindoy LF (1975) *Inorg Chem* 14:1322–1326
47. Wang F, Chen H, Parsons S, Oswald ID, Davidson JE, Sadler PJ (2003) *Chem Eur J* 9:5810–5820
48. Bancroft DP, Lepre CA, Lippard SJ (1990) *J Am Chem Soc* 112:6860–6871
49. Miller SE, House DA (1989) *Inorg Chim Acta* 161:131–137
50. Batchelor LK, Păunescu E, Soudani M, Scopelliti R, Dyson PJ (2017) *Inorg Chem* 56:9617–9633
51. Mendoza-Ferri MG, Hartinger CG, Eichinger RE, Stolyarova N, Severin K, Jakupec MA, Nazarov AA, Keppler BK (2008) *Organometallics* 27:2405–2407

Publisher's Note Springer Nature remains neutral with regard to jurisdictional claims in published maps and institutional affiliations.